

Pressure-Induced Superconductivity in Pr₄Ni₃O₁₀ Single Crystals

Cuiying Pei^{1#}, Mingxin Zhang^{1,2#}, Di Peng^{3,4#}, Shangxiong Huangfu^{5#}, Shihao Zhu¹, Qi Wang^{1,6}, Juefei Wu¹, Zhenfang Xing^{3,4}, Lili Zhang⁷, Yulin Chen^{1,5,8}, Jinkui Zhao², Wenge Yang^{3,4}, Hongli Suo^{5*}, Hanjie Guo^{2*}, Qiaoshi Zeng^{3,4*} and Yanpeng Qi^{1,6,9*}

1. School of Physical Science and Technology, ShanghaiTech University, Shanghai 201210, China
2. Songshan Lake Materials Laboratory, Dongguan 523808, Guangdong, China
3. Center for High Pressure Science and Technology Advanced Research, Shanghai 201203, China
4. Shanghai Key Laboratory of Material Frontiers Research in Extreme Environments (MFree), Institute for Shanghai Advanced Research in Physical Sciences (SHARPS), Shanghai 201203, China
5. Key Laboratory of Advanced Functional Materials, Ministry of Education, College of Materials Science and Engineering, Beijing University of Technology, Beijing, 100124, China
6. ShanghaiTech Laboratory for Topological Physics, ShanghaiTech University, Shanghai 201210, China
7. Shanghai Synchrotron Radiation Facility, Shanghai Advanced Research Institute, Chinese Academy of Sciences, Shanghai 201203, China
8. Department of Physics, Clarendon Laboratory, University of Oxford, Parks Road, Oxford OX1 3PU, UK
9. Shanghai Key Laboratory of High-resolution Electron Microscopy, ShanghaiTech University, Shanghai 201210, China

These authors contributed to this work equally.

* Correspondence should be addressed to Y.P.Q. (qiyp@shanghaitech.edu.cn) or Q.S.Z. (zengqs@hpstar.ac.cn) or H.J.G. (hjguo@sslabor.org.cn) or H.L.S. (honglisuo@bjut.edu.cn)

The recent discovery of superconductivity in pressurized Ruddlesden-Popper (RP) of nickelates has potential similarities with cuprate superconductors, which may provide unique perspectives on the mechanisms of high-temperature superconductivity. Up to now, most of high-pressure experiments concentrated on the lanthanum-related RP phase. Therefore, the discovery of new superconducting nickelate compounds is highly desired to explore the generality of pressure-induced superconductivity in RP nickelates. Here, we grow high-quality $\text{Pr}_4\text{Ni}_3\text{O}_{10}$ single crystal with an optical floating zone furnace under high oxygen pressure and conduct high-pressure transport measurements with various pressure transmitting mediums. The density wave in $\text{Pr}_4\text{Ni}_3\text{O}_{10}$ single crystal was suppressed by pressure, accompanying the arising of superconducting state beyond 10 GPa. The maximum and unsaturated T_c of 39 K is obtained within our research pressure. Although zero resistivity was not achieved in our experiments, the pressure and temperature-dependent diamagnetism along with the systematic evolution of resistivity with applied magnetic field, corroborate the superconductivity in $\text{Pr}_4\text{Ni}_3\text{O}_{10}$ single crystals. Our findings provide a new platform for the investigation of the relationship among structural evolution, magnetism, correlation, and superconductivity in Ruddlesden-Popper nickelates.

Superconductors possessing high superconducting transition temperatures (T_c) remain a long-thought goal within the field of condensed-matter physics. In addition to cuprates¹⁻⁵ and hydrides⁶⁻¹⁰, $\text{La}_3\text{Ni}_2\text{O}_7$ ¹¹ is one of the few superconductors with T_c above the liquid nitrogen temperature (77 K), which opened up the era of nickel-based high-temperature superconductivity.¹²⁻³² Several groups reported superconductivity in $\text{La}_3\text{Ni}_2\text{O}_7$, and subsequently, zero resistance, the hallmark of superconductors, was achieved under hydrostatic pressure conditions improved by a liquid even gas pressure transmitting medium. Recent multislice electron ptychography (MEP) and electron energy loss spectroscopy (EELS) results demonstrated the off-stoichiometry oxygen vacancies not only exist on the inner apical sites but also exhibit spatial fluctuation, which should be responsible for the inhomogeneity of single crystal samples and low superconducting volume fraction observed in previous measurements.³³ Moreover,

since the narrow stability window of oxygen pressures required for growing $\text{La}_3\text{Ni}_2\text{O}_7$ in a floating zone furnace, obtaining high-quality single crystals remains a significant challenge.

In high-temperature cuprate superconductors, the superconducting transition temperature (T_c) depends on the number of CuO_2 planes in the structural unit, and the maximum T_c is realized in the trilayer system. Given its structural similarity to cuprate, it is highly desired to explore higher T_c in trilayer nickelates. Recently our group and several others have reported evidence of superconductivity in the trilayer phase of $\text{La}_4\text{Ni}_3\text{O}_{10}$ single crystals under pressure,³⁴⁻⁴⁰ However, the maximum T_c of 30 K is much lower than that of the bilayer phase. Nevertheless, superconductivity in $\text{La}_4\text{Ni}_3\text{O}_{10}$, where the formal valence $\text{Ni}^{2.67+}$ instead of $\text{Ni}^{2.5+}$ in $\text{La}_3\text{Ni}_2\text{O}_7$, demonstrates that superconductivity is stable across a range of nickel charge concentrations. On the other hand, intralayer and interlayer couplings and pairings can be modulated in nickelates by adjusting the stacking layers. The pairing frustration effect in pressurized $\text{La}_4\text{Ni}_3\text{O}_{10}$ leads to a much lower T_c than that in pressurized $\text{La}_3\text{Ni}_2\text{O}_7$ single crystals.⁴¹

Recently, the observation of superconductivity at 82.5 K, accompanied by distinct diamagnetic signals, was reported in a Pr-doped $\text{La}_2\text{PrNi}_2\text{O}_7$ polycrystal under high pressure.¹³ The introduction of Pr not only amplified orthorhombic structural distortions but also induced valence instability at elevated temperatures. Inspired by the above work, a question arises naturally: is it possible to achieve superconductivity in Pr-based RP nickelates? To address this, we synthesized the trilayer nickelate $\text{Pr}_4\text{Ni}_3\text{O}_{10}$ single crystal and performed a series of transport measurements under high pressure. An obvious signal of density wave was suppressed by pressure, and we found pressure-induced superconductivity with an unsaturated T_c of 39 K at 72.5 GPa. A distinct diamagnetic transition was observed at 30 GPa, corroborating the presence of superconductivity. Synchrotron X-ray diffraction (XRD) measurements were employed to illustrate the structural evolution of $\text{Pr}_4\text{Ni}_3\text{O}_{10}$ under high pressure. Combining the electrical transport measurements using different pressure transmitting mediums (PTM), we have constructed a T - P phase diagram.

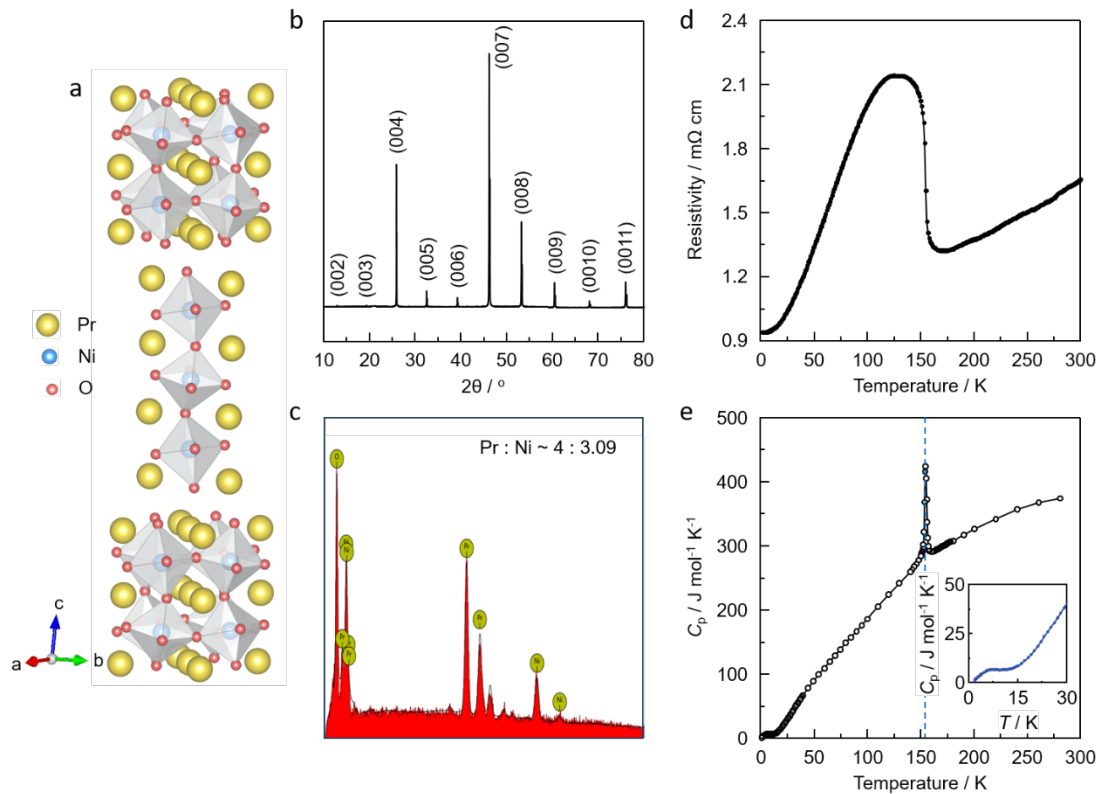


Figure 1. (a) Crystal structure of $\text{Pr}_4\text{Ni}_3\text{O}_{10}$. (b) The room temperature x-ray diffraction peaks from the ab plane of $\text{Pr}_4\text{Ni}_3\text{O}_{10}$ single crystal. (c) The stoichiometry of $\text{Pr}_4\text{Ni}_3\text{O}_{10}$ single crystal measured by the energy dispersive spectroscopy (EDS) spectrum. (d) Temperature-dependence of ab -plane resistivity $\rho(T)$ of $\text{Pr}_4\text{Ni}_3\text{O}_{10}$ single crystal. (e) Temperature-dependent heat capacity of $\text{Pr}_4\text{Ni}_3\text{O}_{10}$ single crystal.

$\text{Pr}_4\text{Ni}_3\text{O}_{10}$, a member of the Ruddlesden-Popper trilayer rare-earth-nickelates, is constructed by stacking of perovskite $(\text{PrNiO}_3)_3$ blocks and rock salt PrO layers along the c axis (Figure 1a). It crystallizes in the space group of $P2_1/a$ with distorted NiO_6 octahedra. As reported, $\text{Pr}_4\text{Ni}_3\text{O}_{10}$ nominally contains $\text{Ni}^{2+}/\text{Ni}^{3+}$, with an average valence state of 2.67^+ ,⁴² which gives rise to strongly coupled electronic and magnetic phases. The $\text{Pr}_4\text{Ni}_3\text{O}_{10}$ single crystal was successfully grown using an optical floating zone furnace under an oxygen pressure of 140-150 bar.^{42,43} Figure 1b shows the XRD peaks from the ab plane of $\text{Pr}_4\text{Ni}_3\text{O}_{10}$ single crystal at room temperature. All peaks can be well indexed by the (00l) reflections of $\text{Pr}_4\text{Ni}_3\text{O}_{10}$. The compositions derived from a typical energy dispersive spectroscopy (EDS) measurement on the crystal reveal a good stoichiometry with an atomic ratio of $\text{Pr} : \text{Ni} = 4 : 3.09$. (Figure 1c) The XRD and EDS results collectively confirm the high quality of $\text{Pr}_4\text{Ni}_3\text{O}_{10}$ single crystals.

Prior to high-pressure measurements, we carried out transport measurements at ambient pressure. The temperature-dependent resistivity of the as-grown $\text{Pr}_4\text{Ni}_3\text{O}_{10}$ single crystal is depicted in Figure 1d. The resistivity decreases with decreasing temperature, displaying a metallic behavior. A distinct steplike kink is observed in the resistivity curve at around 156 K. This anomaly resembles the situation in $\text{La}_4\text{Ni}_3\text{O}_{10}$, suggesting the emergence of a density wave state, as previously demonstrated in neutron diffraction experiments.³⁸ The heat capacity of $\text{Pr}_4\text{Ni}_3\text{O}_{10}$ is illustrated in Figure 1e. A sharp peak at 156 K indicates a phase transition. The anomaly below 10 K could be attributed to magnetic ordering from Pr ions.⁴⁴ Temperature-dependent in-plane (B_{\parallel}) and out-of-plane (B_{\perp}) magnetic properties were measured on $\text{Pr}_4\text{Ni}_3\text{O}_{10}$ single crystal under a magnetic field of 0.4 T. (Figure S1) An anomaly is clearly seen in $d\chi/dT$ at 156 K, consistent with the kink in resistivity and heat capacity. In contrast to $\text{La}_4\text{Ni}_3\text{O}_{10}$, an anomaly is also observed around 6 K, indicating the magnetic nature of $\text{Pr}_4\text{Ni}_3\text{O}_{10}$. The phase transition observed in our measurements is considerably sharper than previously reported results, indicating the high quality of our $\text{Pr}_4\text{Ni}_3\text{O}_{10}$ single crystals.

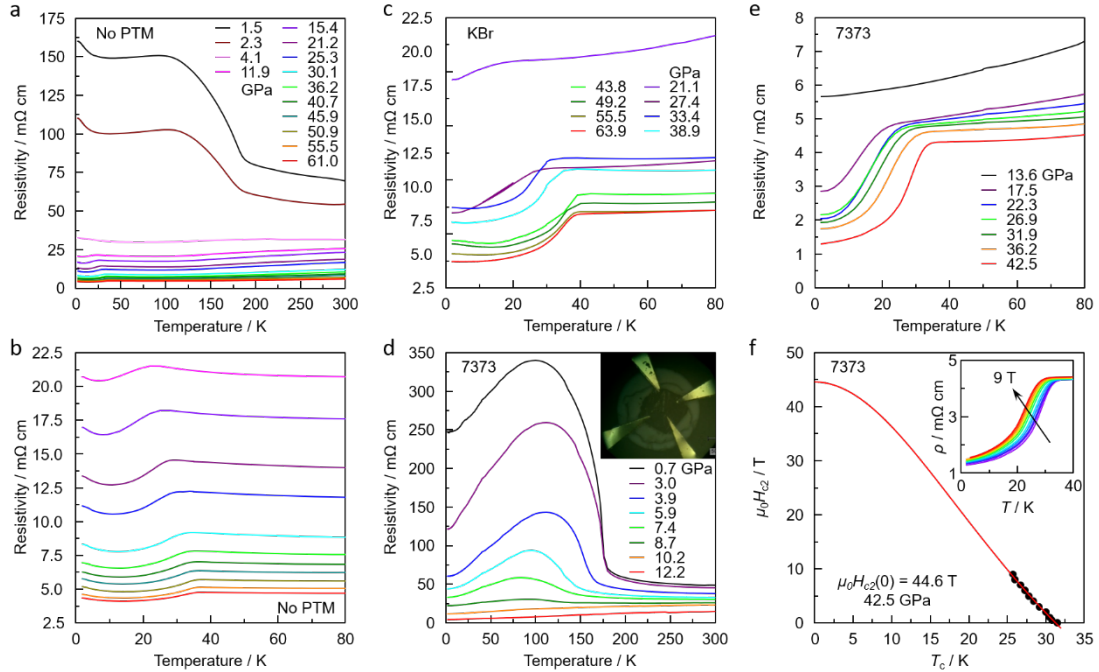


Figure 2. (a) Electrical resistivity $\rho(T)$ of $\text{Pr}_4\text{Ni}_3\text{O}_{10}$ as a function of temperature at different pressures without PTM. (b) Enlarged $\rho(T)$ curves in the vicinity of the superconducting transition without PTM. (c) Enlarged electrical resistivity $\rho(T)$ of $\text{Pr}_4\text{Ni}_3\text{O}_{10}$ as a function of temperature at different pressures with KBr as PTM. (d) Electrical resistivity $\rho(T)$ of $\text{Pr}_4\text{Ni}_3\text{O}_{10}$ as a function of temperature at different pressures

with Daphne 7373 as PTM. (e) Enlarged $\rho(T)$ curves in the vicinity of the superconducting transition with Daphne 7373 as PTM. (f) Temperature dependence of the upper critical field $\mu_0 H_{c2}(T)$ with Daphne 7373 as PTM. The insert is electrical resistivity $\rho(T)$ under various magnetic fields at 42.5 GPa with Daphne 7373 as PTM. Here the T_c are determined at 90% of the normal state resistivity just above the onset superconducting transition temperature. The red solid lines represent the fits using the Ginzburg-Landau formula.

The temperature-dependent resistivity of $\text{Pr}_4\text{Ni}_3\text{O}_{10}$ at various pressures is presented in Figure 2. Without PTM, the resistivity increases with decreasing temperature below 300 K, exhibiting a weak insulating behavior (Figure 2a). A distinctive kink in the resistivity curve manifests at the charge ordering temperature. The upturn in resistivity at low temperatures is potentially associated with antiferromagnetic order in the Pr sublattice. With pressure increasing, the anomalous resistivity associated with the density wave is suppressed, followed by metallization. Subsequently, a small drop at 20 K in resistivity becomes noticeable at 11.9 GPa, indicating the emergence of a superconducting transition. With further compression, the resistivity drop becomes more pronounced. The superconducting T_c rises with increasing pressure and does not show signs of saturation. It should be noted that the upturn in resistivity below 25 K persists throughout the entire pressure range, and the critical temperature initially decreases in the weak insulator region before reversing after metallization.

To improve the hydrostatic condition within the DAC chamber, we utilized KBr as the PTM for high-pressure transport measurements. As shown in Figure 2c, the weak insulator behavior and non-monotonic changes in resistivity with a density wave are reproducible. However, the resistivity upturn around 20 K becomes inconspicuous. As pressure increases, the density wave is suppressed, and metallization is restored at a relatively higher pressure. Above 21 GPa, a drop in the resistivity curve occurs around 20 K. With further increases in pressure, the onset of the superconducting transition rises and reaches a plateau at 39 K.

We also conducted the high-pressure temperature-dependent resistivity measurements using Daphne 7373 as the PTM to further improve the hydrostatic

condition. As shown in Figures 2d and 2e, we observed a steplike kink in the resistivity similar to that at ambient pressure. With pressure increasing, the characteristic kink attributed to density wave was suppressed, and the critical temperature continued to decrease. Eventually, the resistivity exhibits a metallic behavior at around 10 GPa. With further increments in pressure, a drop in the resistivity below 20 K was observed at 17.5 GPa. The T_c increases with pressure and still does not exhibit the trend of saturation. It should be noted that the superconducting transition becomes more unambiguous with liquid PTM. Despite our experiment has not achieved zero resistivity state until 42.5 GPa, a larger resistivity drop of 70% was achieved for the $\text{Pr}_4\text{Ni}_3\text{O}_{10}$ sample.

To further confirm the pressure-induced superconductivity, we performed electrical resistivity measurements under various magnetic fields at 42.5 GPa. As illustrated in Figure 2f, the resistivity drop is progressively suppressed under magnetic field, shifting to approximately 25 K at 9 T. This behavior further corroborates that the resistivity drop originates from a superconducting transition. We estimated the upper critical field $\mu_0 H_{c2}(T)$ by fitting it with the empirical Ginzburg-Landau formula $\mu_0 H_{c2}(T) = \mu_0 H_{c2}(0)(1 - t^2)/(1 + t^2)$, where $t = T/T_c$. The fitted zero-temperature upper critical field $\mu_0 H_{c2}(0)$ of $\text{Pr}_4\text{Ni}_3\text{O}_{10}$, derived from the 90% resistivity of the normal state around T_c , reaches 44.6 T with $T_c = 31.3$ K at 42.5 GPa. When using KBr as PTM, it yields 53.8 T with $T_c = 34.7$ K at 63.9 GPa. (Figure S2) It should be noted that the $\mu_0 H_{c2}(0)$ obtained here is lower than its corresponding Pauli paramagnetic limit $H_P = 1.84T_c$. According to the relationship $\mu_0 H_{c2} = \Phi_0/(2\pi\xi^2)$, where $\Phi_0 = 2.07 \times 10^{-15}$ Wb is the flux quantum, the Ginzburg-Landau coherence length $\xi_{\text{GL}}(0)$ is 2.72 nm at 42.5 GPa and 2.48 nm at 63.9 GPa, respectively.

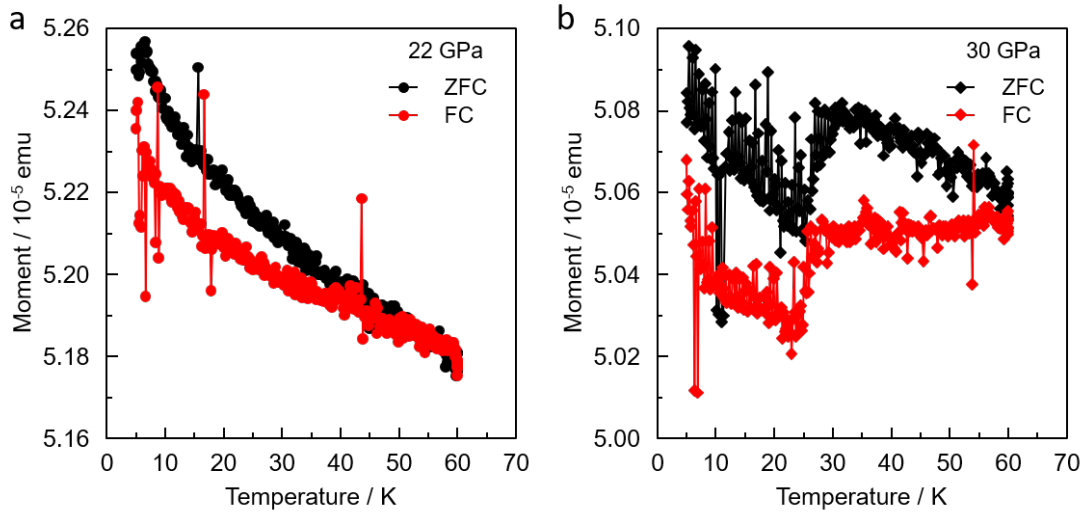


Figure 3. Temperature-dependent magnetization of $\text{Pr}_4\text{Ni}_3\text{O}_{10}$ under a magnetic field of 5 Oe using the zero-field-cooled (ZFC) and field-cooled (FC) modes at 22 GPa and 30 GPa, respectively.

To further validate the pressure-induced superconductivity, we conducted ultrasensitive direct current (d.c.) magnetic susceptibility measurements under high pressures using a custom-built miniature beryllium-copper alloy DAC. This approach could observe the Meissner effect of superconductivity. Analysis of the high-pressure d.c. susceptibility data revealed no obvious transition in either the zero-field-cooled (ZFC) or field-cooled (FC) modes at 22 GPa. (Figure 3) However, upon increasing the pressure to 30 GPa, a distinct diamagnetic transition was observed in both the ZFC and FC measurements, which provides direct evidence of the superconducting Meissner effect. At this pressure, the superconducting transition temperature derived from magnetic measurements is consistent with the results obtained from electrical transport measurements, providing further evidence for the superconductivity.

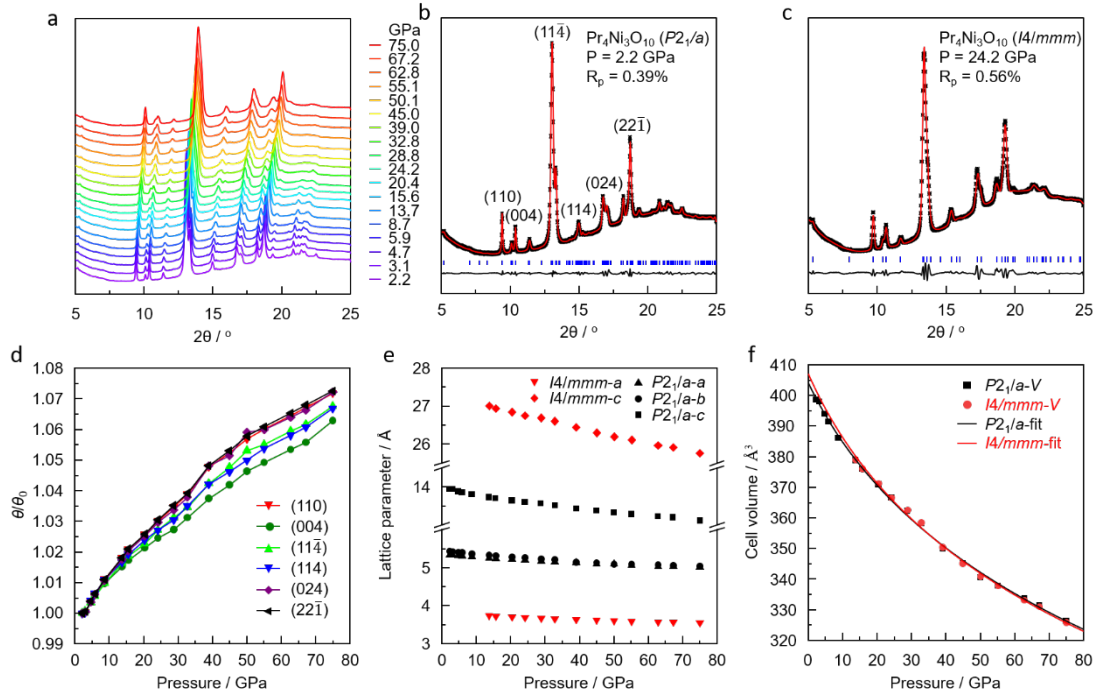


Figure 4. (a) XRD patterns of $\text{Pr}_4\text{Ni}_3\text{O}_{10}$ measured at room temperature with external pressure increase up to 75.0 GPa. The X-ray wavelength λ is 0.6199 Å. (b) Typical Rietveld refinement of $\text{Pr}_4\text{Ni}_3\text{O}_{10}$ at 2.2 GPa. The experimental and calculated patterns are indicated by black stars and red lines, respectively. The solid lines shown at the bottom of the figures are the residual intensities. The vertical bars indicate the peak positions of the Bragg reflections for $\text{Pr}_4\text{Ni}_3\text{O}_{10}$ in $P2_1/a$ space group. (c) Typical Rietveld refinement of $\text{Pr}_4\text{Ni}_3\text{O}_{10}$ at 24.2 GPa. The experimental and calculated patterns are indicated by black stars and red lines, respectively. The solid lines shown at the bottom of the figures are the residual intensities. The vertical bars indicate the peak positions of the Bragg reflections for $\text{Pr}_4\text{Ni}_3\text{O}_{10}$ in $I4/mmm$ space group. (d) Evolution of the (110), (004), $(11\bar{4})$, (114), (024) and $(22\bar{1})$ peak positions under pressure extracted from the Rietveld refinement results. (e) Pressure dependence of lattice parameters a , b and c for $\text{Pr}_4\text{Ni}_3\text{O}_{10}$ in $P2_1/a$ (black) and $I4/mmm$ (red) space group extracted from the synchrotron XRD results. (f) Pressure dependence of volume for $\text{Pr}_4\text{Ni}_3\text{O}_{10}$ in $P2_1/a$ (black) and $I4/mmm$ (red) space group, respectively. A third-order Birch-Murnaghan equation of state fitting by $P2_1/a$ phase is from 2.2 GPa to 75.0 GPa, while it is from 13.7 GPa to 75.0 GPa for $I4/mmm$ phase.

To elucidate the structural evolution of $\text{Pr}_4\text{Ni}_3\text{O}_{10}$ under high pressure, we performed *in situ* synchrotron XRD measurements on powdered $\text{Pr}_4\text{Ni}_3\text{O}_{10}$ single crystals under various pressures. As shown in Figure 4a, all the diffraction peaks in the low-pressure range align well with the structure observed at ambient pressure. The Rietveld refinement corroborates a monoclinic structure with the $P2_1/a$ space group. As

illustrated in Figure 4b, the refinements of $\text{Pr}_4\text{Ni}_3\text{O}_{10}$ at 2.2 GPa converged effectively with reliable factors $R_p = 0.39\%$, thereby confirming the phase purity and high quality of our crystals.

We further refined all XRD data up to the maximum experimental pressure of 75.0 GPa and found that all the diffraction patterns can be indexed well with the $P2_1/a$ phase. The refinement reliable factors did not exceed 0.42% as detailed in Table S1. All the a , b and c lattice parameters show a monotonical decrease with increasing pressure, as depicted in Figure 4e. The lattice parameters of $\text{Pr}_4\text{Ni}_3\text{O}_{10}$ under various pressures are smaller than those of $\text{La}_4\text{Ni}_3\text{O}_{10}$ ^{34,45} due to the chemical pre-compression effect caused by the smaller Pr in lattice (Figure S3). We extracted and plotted the trend of peak positions as a function of pressure based on refinement results. As shown in Figure 4d, the evolution of (110), (004), ($11\bar{4}$), (114), (024), and ($22\bar{1}$) peak positions do not exhibit significant changes under high pressure. According to previous reports^{38,45}, $\text{La}_4\text{Ni}_3\text{O}_{10}$ single crystal undergo a pressure-induced structural phase transition from $P2_1/a$ to $I4/mmm$ at around 15 GPa. We performed Rietveld refinement with an $I4/mmm$ structure on XRD patterns with pressure from 13.7 GPa to 75.0 GPa. In this case, the refinement converged to $R_p = 0.78\%$ for $I4/mmm$ at 13.7 GPa. As shown in Figure 4c, there is significant residual intensity next to the main diffraction peaks. With pressure increasing, the refinement reliable factors decrease but remain above 0.48%. The refined unit-cell parameters and volume of $\text{Pr}_4\text{Ni}_3\text{O}_{10}$ with $I4/mmm$ phase are displayed in Figures 4e and 4f. A third-order Birch-Murnaghan equation of state was used to fit the measured pressure-volume (P - V) data (Figure 4f) for two phases of $\text{Pr}_4\text{Ni}_3\text{O}_{10}$ in different pressure ranges. The bulk modulus, K_0 , is 175.0 ± 15.0 GPa with $V_0 = 404.1 \pm 1.4$ Å³ and $K'_0 = 6.6 \pm 0.8$ for $\text{Pr}_4\text{Ni}_3\text{O}_{10}$ in $P2_1/a$ phase fitting from 2.2 GPa to 75.0 GPa. Whereas it is $K_0 = 159.6 \pm 43.2$ GPa with $V_0 = 407.0 \pm 5.7$ Å³ and $K'_0 = 7.0 \pm 1.9$ when $\text{Pr}_4\text{Ni}_3\text{O}_{10}$ is in $I4/mmm$ phase with pressure from 13.7 GPa to 75.0 GPa. Notably, the difference between $P2_1/a$ and $I4/mmm$ phase is subtle. Consequently, further experiments are needed to confirm the existence of pressure-induced structural phase transition in $\text{Pr}_4\text{Ni}_3\text{O}_{10}$ single crystals.

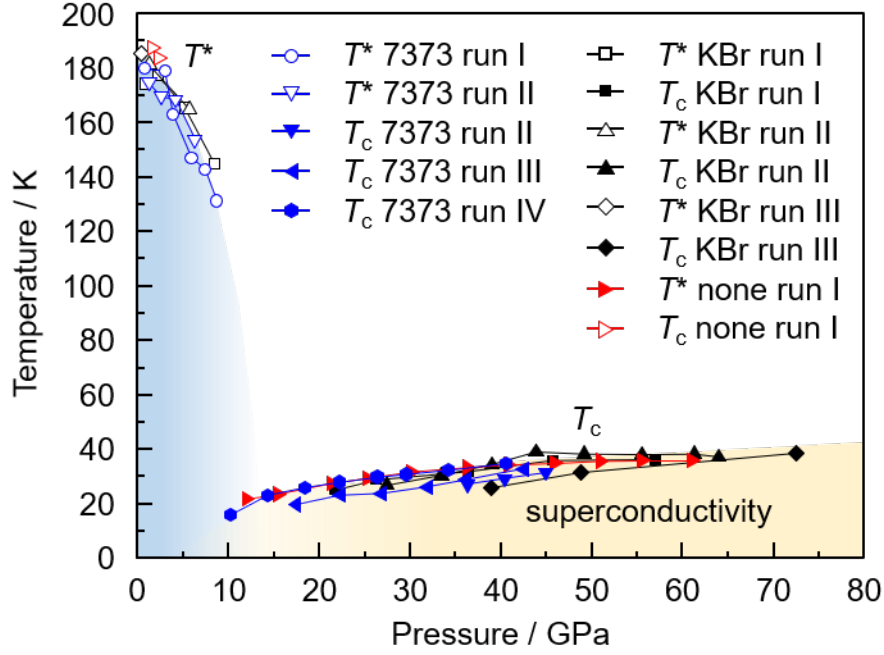


Figure 5. Pressure dependence of the superconducting transition temperatures T_c s and density wave transition temperature T^* s for $\text{Pr}_4\text{Ni}_3\text{O}_{10}$.

Based on the above electrical transport measurements under pressure, the T - P phase diagram is summarized in Figure 5. Here, we performed high-pressure measurements in DAC with non-PTM and using solid (KBr) or liquid (Daphne 7373) as PTM. Several independent runs on different $\text{Pr}_4\text{Ni}_3\text{O}_{10}$ single crystals yielded consistent and reproducible results. In the lower pressure region, $\text{Pr}_4\text{Ni}_3\text{O}_{10}$ undergoes two transitions, forming the intertwined density wave on the Ni sublattice and the magnetic order on the Pr sublattice. The density wave, which manifests as an anomaly in resistivity at 180 K, was observed to be suppressed under pressure. A superconducting state emerges beyond a critical pressure of 10 GPa. The T_c increases dramatically with pressure and a maximum and unsaturated T_c of 39 K is obtained within the limit of our research. Considering the similarity of the synchrotron XRD patterns under various pressures, our data at present cannot conclusively demonstrate whether the emergence of high-temperature superconductivity is derived from a structural phase transition. Hence, the origin of pressure-induced high-temperature superconducting phase in $\text{Pr}_4\text{Ni}_3\text{O}_{10}$ remains an open question.

The maximum T_c of 39 K observed in $\text{Pr}_4\text{Ni}_3\text{O}_{10}$ is higher than that of $\text{La}_4\text{Ni}_3\text{O}_{10}$,

which resembles the situation in iron-based superconductivity $\text{PrFeAsO}_{1-x}\text{F}_x$ ⁴⁶. The enhancement of T_c could mainly be attributed to pre-compression of the unit cell after substitution of La with Pr. The pressure and temperature-dependent diamagnetism together with systematic evolution of resistivity with applied magnetic field corroborate the observation of superconductivity in $\text{Pr}_4\text{Ni}_3\text{O}_{10}$. However, zero resistivity was not achieved in our high-pressure measurements. Unlike the case of $\text{La}_4\text{Ni}_3\text{O}_{10}$, Pr^{3+} ions build the interlayer exchange pathways to develop a spin density wave ground state at lower temperatures.⁴⁷ The suppression of the Ni sublattice density wave naturally diminished the exchange field felt by the Pr^{3+} sites, however, our magnetic susceptibility data at 30 GPa show an obvious increase below 10 K. We assume that the static long-range magnetic order in the Pr sublattice in $\text{Pr}_4\text{Ni}_3\text{O}_{10}$ single crystal plays a nonnegligible effect on superconductivity. Further experiments are needed to explore whether Pr^{3+} in $\text{Pr}_4\text{Ni}_3\text{O}_{10}$ under pressure adopts a non-magnetic singlet ground state.

In conclusion, we have successfully grown high-quality single crystals of $\text{Pr}_4\text{Ni}_3\text{O}_{10}$ and performed a series of transport measurements at high pressure. The superconducting state emerges after the suppression of the density wave. The T_c increases dramatically with pressure and a maximum and unsaturated T_c of 39 K is obtained within the limit of our research. The discovery of superconductivity in $\text{Pr}_4\text{Ni}_3\text{O}_{10}$ single crystals not only broadens the family of RP nickelate superconductors, but also provides an ideal platform for exploring the relationship between density wave, magnetic order, and high-temperature superconductivity.

Note added: While preparing this paper, we also noted two related studies that reported resistance measurements on $\text{Pr}_4\text{Ni}_3\text{O}_{10}$ polycrystalline and single crystal samples.^{45,48} Most results are similar to ours. Zero resistance was also not achieved in these parallel works, which indicates small superconducting volume fractions.

Acknowledgements

This work was supported by the National Natural Science Foundation of China (Grant Nos. 52272265, 12474018) and the National Key R&D Program of China (Grant No. 2023YFA1607400). Q.S.Z., D.P. and W.Y. acknowledge the support from the

National Natural Science Foundation of China (Grant Nos. 51871054, 52101187) and Shanghai Key Laboratory of Material Frontiers Research in Extreme Environments, China (Grant No. 22dz2260800), the Shanghai Science and Technology Committee, China (Grant No. 22JC1410300). H.J.G acknowledges the support from the National Natural Science Foundation of China (Grant No. 12004270) and Guangdong Basic and Applied Basic Research Foundation (Grant No. 2022B1515120020). S.H. acknowledges the Beijing Postdoctoral Research Foundation (2024-ZZ-023). H.L.S. acknowledges the National Natural Science Foundation of China (Grant No. 52277021). The authors thank the support from Analytical Instrumentation Center (# SPSTAIC10112914), SPST, ShanghaiTech University. The authors thank the staff members at BL15U1 in Shanghai Synchrotron Radiation Facility for assistance during data collection.

Competing interests

The authors declare no competing interests.

References

- 1 Schilling, A., Cantoni, M., Guo, J. D. & Ott, H. R. Superconductivity above 130 K in the Hg-Ba-Ca-Cu-O system. *Nature* **363**, 56, (1993).
- 2 Gao, L. *et al.* Superconductivity up to 164 K in $\text{HgBa}_2\text{Ca}_{m-1}\text{Cu}_m\text{O}_{2m+2+\delta}$ ($m=1, 2, \text{ and } 3$) under quasihydrostatic pressures. *Phys. Rev. B* **50**, 4260-4263, (1994).
- 3 Scott, B. A. *et al.* layer dependence of the superconducting transition temperature of $\text{HgBa}_2\text{Ca}_{n-1}\text{Cu}_n\text{O}_{2n+2+\delta}$. *Physica C Supercond.* **230**, 239-245, (1994).
- 4 Kuzemskaya, I. G., Kuzemsky, A. L. & Cheglokov, A. A. superconducting properties of the family of mercurocuprates and role of layered structure. *Low-Temp. Phys.* **118**, 147-152, (2000).
- 5 Iyo, A. *et al.* T_c vs n relationship for multilayered high- T_c superconductors. *J. Phys. Soc. Jpn.* **76**, 094711, (2007).
- 6 Drozdov, A. P. *et al.* Superconductivity at 250 K in lanthanum hydride under high pressures. *Nature* **569**, 528-531, (2019).
- 7 Somayazulu, M. *et al.* Evidence for superconductivity above 260 K in lanthanum superhydride at megabar pressures. *Phys. Rev. Lett.* **122**, 027001, (2019).
- 8 Ma, L. *et al.* High-temperature superconducting phase in clathrate calcium hydride CaH_6 up to 215 K at a pressure of 172 GPa. *Phys. Rev. Lett.* **128**, 167001, (2022).
- 9 Chen, W. *et al.* High-temperature superconducting phases in cerium superhydride with a T_c up to 115 K below a pressure of 1 Megabar. *Phys. Rev. Lett.* **127**, 117001, (2021).
- 10 Li, Z. *et al.* Superconductivity above 200 K discovered in superhydrides of calcium. *Nat.*

- Commun.* **13**, 2863, (2022).
- 11 Sun, H. *et al.* Signatures of superconductivity near 80 K in a nickelate under high pressure. *Nature* **621**, 493-498, (2023).
- 12 Zhang, Y. *et al.* High-temperature superconductivity with zero resistance and strange-metal behaviour in $\text{La}_3\text{Ni}_2\text{O}_{7-\delta}$. *Nat. Phys.* **20**, 1269-1273, (2024).
- 13 Wang, N. *et al.* Bulk high-temperature superconductivity in pressurized tetragonal $\text{La}_2\text{PrNi}_2\text{O}_7$. *Nature* **634**, 579-584, (2024).
- 14 Liu, Z. *et al.* electronic correlations and energy gap in the bilayer nickelate $\text{La}_3\text{Ni}_2\text{O}_7$. *Nat. Commun.* **15**, 7570, (2024).
- 15 Zhang, M. *et al.* Effects of pressure and doping on Ruddlesden-Popper phases $\text{La}_{n+1}\text{Ni}_n\text{O}_{3n+1}$. *J. Mater. Sci. Technol.* **185**, 147-154, (2024).
- 16 Li, Y. *et al.* Distinct ultrafast dynamics of bilayer and trilayer nickelate superconductors regarding the density-wave-like transitions. *Sci. Bull.*, 10.1016/j.scib.2024.1010.1011, (2024).
- 17 Li, Y. *et al.* Electronic Correlation and Pseudogap-Like Behavior of High-Temperature Superconductor $\text{La}_3\text{Ni}_2\text{O}_7$. *Chinese Phys. Lett.* **41**, 087402, (2024).
- 18 Zhou, Y. *et al.* investigations of key issues on the reproducibility of high T_c superconductivity emerging from compressed $\text{La}_3\text{Ni}_2\text{O}_7$ *arXiv: 2311.12361*, (2023).
- 19 Luo, Z., Hu, X., Wang, M., Wú, W. & Yao, D.-X. Bilayer two-orbital model of $\text{La}_3\text{Ni}_2\text{O}_7$ under pressure. *Phys. Rev. Lett.* **131**, 126001, (2023).
- 20 Christiansson, V., Petocchi, F. & Werner, P. Correlated electronic structure of $\text{La}_3\text{Ni}_2\text{O}_7$ under pressure. *Phys. Rev. Lett.* **131**, 206501, (2023).
- 21 Zhou, X. *et al.* Revealing nanoscale structural phase separation in $\text{La}_3\text{Ni}_2\text{O}_7$ single crystal via scanning near field optical microscopy. *arXiv: 2410.06602*, (2024).
- 22 Zhang, Y., Lin, L.-F., Moreo, A., Maier, T. A. & Dagotto, E. Trends in electronic structures and s_{\pm} -wave pairing for the rare-earth series in bilayer nickelate superconductor $\text{R}_3\text{Ni}_2\text{O}_7$. *Phys. Rev. B* **108**, 165141, (2023).
- 23 Yang, Q.-G., Wang, D. & Wang, Q.-H. Possible s_{\pm} -wave superconductivity in $\text{La}_3\text{Ni}_2\text{O}_7$. *Phys. Rev. B* **108**, L140505, (2023).
- 24 Sakakibara, H. *et al.* Theoretical analysis on the possibility of superconductivity in the trilayer Ruddlesden-Popper nickelate $\text{La}_4\text{Ni}_3\text{O}_{10}$ under pressure and its experimental examination: Comparison with $\text{La}_3\text{Ni}_2\text{O}_7$. *Phys. Rev. B* **109**, 144511, (2024).
- 25 Lu, C., Pan, Z., Yang, F. & Wu, C. Interlayer-coupling-driven high-temperature superconductivity in $\text{La}_3\text{Ni}_2\text{O}_7$ under pressure. *Phys. Rev. Lett.* **132**, 146002, (2024).
- 26 Lu, C., Pan, Z., Yang, F. & Wu, C. Interplay of two E_g orbitals in superconducting $\text{La}_3\text{Ni}_2\text{O}_7$ under pressure. *Phys. Rev. B* **110**, 094509, (2024).
- 27 Liu, Y.-B., Mei, J.-W., Ye, F., Chen, W.-Q. & Yang, F. s_{\pm} -wave pairing and the destructive role of apical-oxygen deficiencies in $\text{La}_3\text{Ni}_2\text{O}_7$ under pressure. *Phys. Rev. Lett.* **131**, 236002, (2023).
- 28 Geisler, B. *et al.* Optical properties and electronic correlations in $\text{La}_3\text{Ni}_2\text{O}_7$ bilayer nickelates under high pressure. *arXiv: 2401.04258*, (2024).
- 29 Zhang, Y., Lin, L.-F., Moreo, A. & Dagotto, E. Electronic structure, dimer physics, orbital-selective behavior, and magnetic tendencies in the bilayer nickelate superconductor

- La₃Ni₂O₇ under pressure. *Phys. Rev. B* **108**, L180510, (2023).
- 30 Shen, Y., Qin, M. & Zhang, G.-M. Effective Bi-layer model hamiltonian and density-matrix renormalization group study for the high-T_c superconductivity in La₃Ni₂O₇ under high pressure. *Chinese Phys. Lett.* **40**, 127401, (2023).
- 31 Wang, M. Discovery of high-T_c superconductivity in a nickelate. *Physics* **52**, 663-671, (2023).
- 32 Wang, M., Wen, H.-H., Wu, T., Yao, D.-X. & Xiang, T. Normal and superconducting properties of La₃Ni₂O₇. *Chinese Phys. Lett.* **41**, 077402, (2024).
- 33 Dong, Z. *et al.* Visualization of oxygen vacancies and self-doped ligand holes in La₃Ni₂O₇ - δ . *Nature* **630**, 847-852, (2024).
- 34 Zhang, M. *et al.* Superconductivity in trilayer nickelate La₄Ni₃O₁₀ under pressure. *arXiv: 2311.07423*, (2023).
- 35 Huo, Z., Zhang, P., Zhang, Z., Duan, D. & Cui, T. Electronic correlations and Hund's rule coupling in trilayer nickelate La₄Ni₃O₁₀. *arXiv: 2407.00327*, (2024).
- 36 Li, J. *et al.* Structural transition, electric transport, and electronic structures in the compressed trilayer nickelate La₄Ni₃O₁₀. *Sci. China Phys. Mech.* **67**, 117403, (2024).
- 37 Fabbris, G. *et al.* Resonant inelastic x-ray scattering data for Ruddlesden-Popper and reduced Ruddlesden-Popper nickelates. *Sci. Data* **10**, 174, (2023).
- 38 Zhu, Y. *et al.* Superconductivity in pressurized trilayer La₄Ni₃O_{10- δ} single crystals. *Nature* **631**, 531-536, (2024).
- 39 Li, Q. *et al.* Signature of superconductivity in pressurized La₄Ni₃O₁₀. *Chinese Phys. Lett.* **41**, 017401, (2024).
- 40 Xu, S. *et al.* Origin of the density wave instability in trilayer nickelate La₄Ni₃O₁₀ revealed by optical and ultrafast spectroscopy. *arXiv: 2405.19161*, (2024).
- 41 Qin, Q., Wang, J. & Yang, Y.-f. Frustrated superconductivity in the trilayer nickelate La₄Ni₃O₁₀. *arXiv: 2405.04340*, (2024).
- 42 Zhang, J. *et al.* High oxygen pressure floating zone growth and crystal structure of the metallic nickelates R₄Ni₃O₁₀ (R=La,Pr). *Phys. Rev. Mater.* **4**, 083402, (2020).
- 43 Huangfu, S. *et al.* Anisotropic character of the metal-to-metal transition in Pr₄Ni₃O₁₀. *Phys. Rev. B* **101**, 104104, (2020).
- 44 Rout, D. *et al.* Structural and physical properties of trilayer nickelates R₄Ni₃O₁₀ (R=La, Pr, and Nd). *Phys. Rev. B* **102**, 195144, (2020).
- 45 Huang, X. *et al.* Signature of superconductivity in pressurized trilayer-nickelate Pr₄Ni₃O_{10- δ} . *arXiv: 2410.07861*, (2024).
- 46 Ren, Z. A. *et al.* Superconductivity at 52 K in iron based F doped layered quaternary compound Pr[O_{1-x}F_x]FeAs. *Mater. Res. Innovations* **12**, 105-106, (2013).
- 47 Samarakoon, A. M. *et al.* Bootstrapped dimensional crossover of a spin density wave. *Phys. Rev. X* **13**, 041018, (2023).
- 48 Chen, X. *et al.* Non bulk superconductivity in Pr₄Ni₃O₁₀ single crystals under pressure. *arXiv: 2410.10666*, (2024).